J Solid State Electrochem (2008) 12:207–211
DOI 10.1007/s10008-007-0364-7

SHORT COMMUNICATION

# Surfactant stabilized nanopetals morphology of $\alpha$-$MnO_2$ prepared by microemulsion method

**S. Devaraj · N. Munichandraiah**

Received: 16 January 2007 / Revised: 15 May 2007 / Accepted: 22 May 2007 / Published online: 21 June 2007


**Abstract** $\alpha$-Manganese dioxide is synthesized in a microemulsion medium by a redox reaction between $KMnO_4$ and $MnSO_4$ in presence of sodium dodecyl sulphate as a surface active agent. The morphology of $MnO_2$ resembles nanopetals, which are spread parallel to the field. The material is further characterized by powder X-ray diffraction, energy dispersive analysis of X-ray, and Brunauer–Emmett–Teller surface area. Supercapacitance property of $\alpha$-$MnO_2$ nanopetals is studied by cyclic voltammetry and galvanostatic charge–discharge cycling. High values of specific capacitance are obtained.

**Keywords** Manganese dioxide · Microemulsion · Nanopetals · Supercapacitor · Cyclic voltammetry

## Introduction

Synthesis of nanomaterials is one of the recent scientific interests in almost all areas of research. Materials of such interest include powders of metals, metal oxides, ceramics, polymers, semiconductors, etc. The shape of nanomaterials is very wide, which include spherical particles, wires, tubes, rods, etc. The experimental conditions of preparation influence the shape, morphology, and properties of nanoscale materials [1]. Two-dimensional nanostructures of materials are rarely reported. Nanowall materials, which are two-dimensional structures, include carbon nanowalls [2, 3], ZnO nanowalls [4], and GaS and GaSe [5]. Besides nanowalls, which generally stand vertically and are interconnected, nanoflower structures are also reported for ZnO [6].

An electrochemical supercapacitor or ultracapacitor is a charge-storage device, which can be used as an energy source for high-power, short pulse applications [7]. Active materials, which are useful for supercapacitors, include high surface area carbon, hydrated ruthenium dioxide, electronically conducting polymers, etc [8]. Although $RuO_2{\cdot}xH_2O$ is extensively investigated owing to its high specific capacitance (about 760 F $g^{-1}$) [9], its high cost is a discouraging factor for practical supercapacitors. Manganese-based compounds are inexpensive, abundant in nature, and environmentally friendly, and therefore, $MnO_2$ is investigated for this purpose [10]. However, specific capacitance of $MnO_2$ is lower (about 165 F $g^{-1}$) than that of $RuO_2{\cdot}xH_2O$ [11]. $MnO_2$ can be prepared by oxidation of $Mn^{2+}$ either by an electrochemical route [12] or a chemical route [13]. Decreasing the particle size is considered to be a significant approach for increasing specific capacitance of $MnO_2$ [14]. Studies reported on synthesis of nanoscale $MnO_2$ and its characterization for capacitor properties are scarce [15]. In the present work, $MnO_2$ is prepared with nanopetals morphology by a redox reaction between $KMnO_4$ and $MnSO_4$ in a microemulsion medium, which consists of sodium dodecyl sulphate as a surface active agent.

## Materials and methods

Analytical grade or high purity chemicals, namely, $KMnO_4$, $MnSO_4{\cdot}H_2O$, cyclohexane, sodium dodecyl sulphate (SDS, all from Merck), *n*-butanol (SD Fine Chemicals), and $Na_2SO_4$ (BDH) were used for the experiments. Solutions were prepared in doubly distilled water. $MnO_2$ was syn-

S. Devaraj · N. Munichandraiah (✉)
Department of Inorganic and Physical Chemistry,
Indian Institute of Science,
Bangalore 560 012, India
e-mail: muni@ipc.iisc.ernet.in

thesized from a quaternary microemulsion consisting of water-cyclohexane-SDS-*n*-butanol. A solution was prepared by mixing 51.2 ml of cyclohexane (oil), 6.2 ml of *n*-butanol (cosurfactant), and 0.45 g of SDS (surfactant) and stirred well until it became optically transparent. The solution was divided into two equal parts. To one part of the nonaqueous medium, 10 ml of aqueous solution of 0.1 M $KMnO_4$ was added, and to the other part, 10 ml of aqueous solution of 0.15 M $MnSO_4{\cdot}H_2O$ was added. Each portion of the emulsion was copiously mixed using a magnetic bar before they were mixed together. The final emulsion was stirred for 12 h to get a dark-brown precipitate. The product was separated and dried at 70 °C for 12 h in air.

For electrochemical characterization, electrodes were prepared on high-purity battery grade Ni foil (0.18 mm thick) as the current collector. A Ni foil of 10 mm width and 80 mm length was sectioned out of a sheet; 2 $cm^2$ area at one end was used to prepare the $MnO_2$-coated electrode, and the rest of its length was used as a tag for electrical connection. The Ni foil was polished with successive grades of emery, cleaned with detergent, washed copiously with doubly distilled water, rinsed with acetone, dried in air, and weighed. $MnO_2$ (70%), acetylene black (20%), and polyvinylidene difluoride (10%) were ground in a mortar; a few drops of 1-methy-2-pyrrolidone was added to form a syrup. It was coated on to the pretreated Ni foil (2 $cm^2$) and dried at 110 °C under vacuum. Coating and drying steps were repeated to get a required loading level of active material (0.5 mg $cm^{-2}$). Finally, the electrodes were dried at 110 °C under vacuum for 12 h. Average thickness of $MnO_2$ coating was about 40 μm, which was measured using a Digitrix Mark II digital micrometer 901-151 EDl-25. A glass cell, which had provision for introducing $MnO_2$-working electrode, Pt auxiliary electrode and a reference electrode were employed for electrochemical studies. A saturated calomel electrode (SCE) was used as the reference electrode, and potential values are reported against SCE. All electrochemical experiments were done at 20±2 °C.

Powder X-ray diffraction (XRD) patterns were recorded using Philips XRD X'PERT PRO diffractometer using $CuK_\alpha$ as a source. Morphology and energy dispersive analysis of X-ray (EDAX) were recorded using FEI Sirion scanning electron microscope (SEM), which was coupled with Oxford Instrument super ultra thin window EDAX. Brunauer–Emmett–Teller (BET) surface area measurements in $N_2$ atmosphere were carried out using SMARTSORB-92/93 surface area analyzer. Sartorious balance of model CP22D-OCE with 10-μg sensitivity was used for weighing electrodes and materials. Electrochemical studies were carried out using a potentiostat/galvanostat EG&G PARC model Versastat II or Solartron model 1286. Thermogravimetric analysis (TGA) was performed for powder $MnO_2$ in the temperature range ambient to 900 °C in air at a heating rate of 10 °C per minute using NETZSCH TG 209 F1 thermogravimetric analyzer.

## Results and discussion

In the present synthetic procedure, manganese dioxide is obtained from both the reactants, namely, $MnSO_4$ and $KMnO_4$. Oxidation of $Mn^{2+}$ by the reduction in $Mn^{7+}$ results in the formation of $Mn^{4+}$ from both the reactant species:

$$3Mn^{2+} + 2Mn^{7+} \rightarrow 5Mn^{4+} \quad (1)$$

$Mn^{4+}$ precipitates as $MnO_2$ in an aqueous medium:

$$Mn^{4+} + 2H_2O \rightarrow MnO_2 + 4H^+ \quad (2)$$

In the reaction medium, which is a microemulsion, the manganese salts are present in the aqueous phase, and the surfactant molecules orient with their polar head group towards the aqueous phase and their nonpolar hydrocarbon chain towards the organic phase [16]. Owing to shielding of surfactant molecules, the reaction zone is limited to the microemulsion. The product, namely $MnO_2$, formed possesses a nanostructure.

SEM micrograph (Fig. 1a) shows that the sample consists of petal-like structures distributed uniformly along with some amorphous-like nanoparticles. High magnification SEM image (Fig. 1b) presents a view of nanopetal surface parallel to the field. Unlike the general belief that nanowalls stand vertically and are interconnected, Fig. 1a shows that nanopetals are distributed parallel to the field with a wide separation. The petal surface is smooth, which spreads 1 to 2 μm in length. A rough estimation of petal thickness provides values of approximately in the range of 100–200 nm. The observation of nanopetals of $MnO_2$ obtained in the present study (Fig. 1a,b) is similar to nanoflowers reported for ZnO [6]. Surface area measurements using $N_2$ adsorption on nanopetals of α-$MnO_2$ powder by BET isotherm provided a value of 119 $m^2\ g^{-1}$.

The samples were subjected to EDAX and XRD studies. The EDAX spectrum (Fig. 1c) indicates the presence of Mn and O as the major elements. Peaks corresponding to C, Na, K, and S are also present. Whereas K is derived from $KMnO_4$, the origin of C, Na, and S is SDS used for synthesis. It is known that $MnO_2$ exhibits polymorphism with α, β, γ, and δ forms, which depend on the conditions of synthesis. The XRD pattern (Fig. 2) was indexed on a tetragonal phase with lattice constants of $a=b=9.802$ Å, $c=2.863$ Å, and unit cell volume 275.075 $Å^3$ in the space group I4/m (JCPDS no: 44-0141). The lattice constants are in agreement with the reported values [15]. The broad XRD peaks (Fig. 2) reflect nanocrystalline nature of the com-

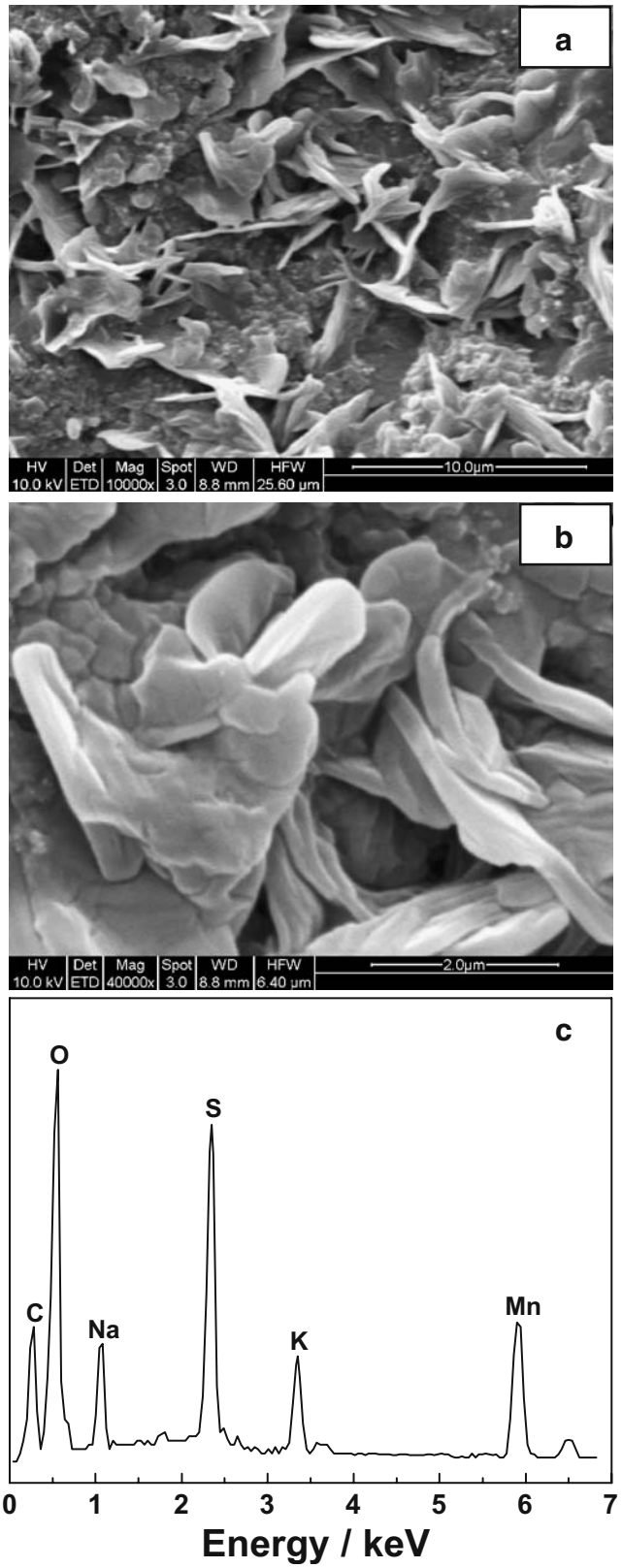


**Fig. 1** SEM micrographs (**a** and **b**) in different magnifications and EDAX spectrum (**c**) of $MnO_2$

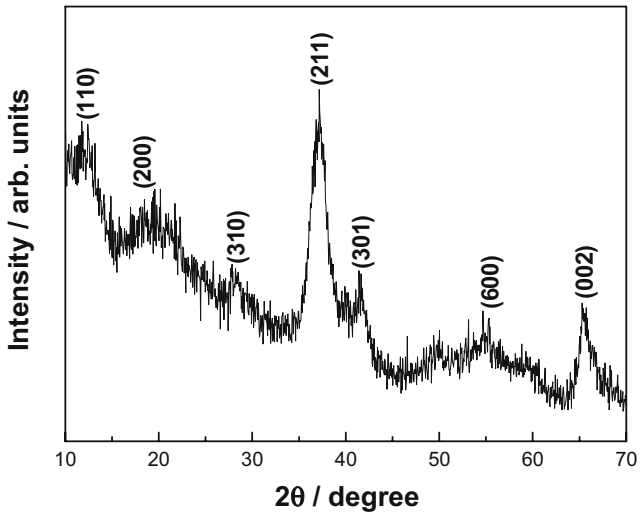


**Fig. 2** XRD pattern of nanopetal $MnO_2$

pound. As the surfactant and potassium salt are present at low concentration, they are not detectable in the XRD studies.

On subjecting the nanopetal α-$MnO_2$ to a thorough washing in methanol and doubly distilled water followed by drying at 70 °C for 12 h, it was found that the nanopetal morphology collapsed, and nanoparticles of spherical morphology resulted as seen in SEM micrograph (Fig. 3). It is thus concluded that the nanopetal morphology of $MnO_2$ is due to the action of surface active molecules. It is likely that the $MnO_2$ particles are aggregated by adsorption of SDS molecules resulting in the morphology of nanopetals.

TGA thermogram of nanopetal $MnO_2$ (Fig. 4) shows 29% weight loss below 260 °C, which corresponds to a loss of water, organic reactants, and trace amount of oxygen. Weight loss of about 4% at around 575 °C corresponds to the loss of oxygen from $MnO_2$ lattice resulting in the phase transformation to $Mn_2O_3$, and another 3% weight loss at 790 °C corresponds to further loss of oxygen resulting in phase transformation from $Mn_2O_3$ to $Mn_3O_4$. The nature of

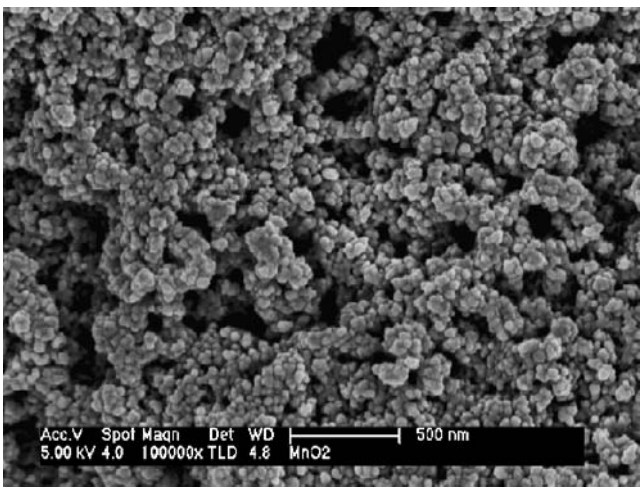


**Fig. 3** SEM micrograph of nanoparticles of α-$MnO_2$ obtained after washing

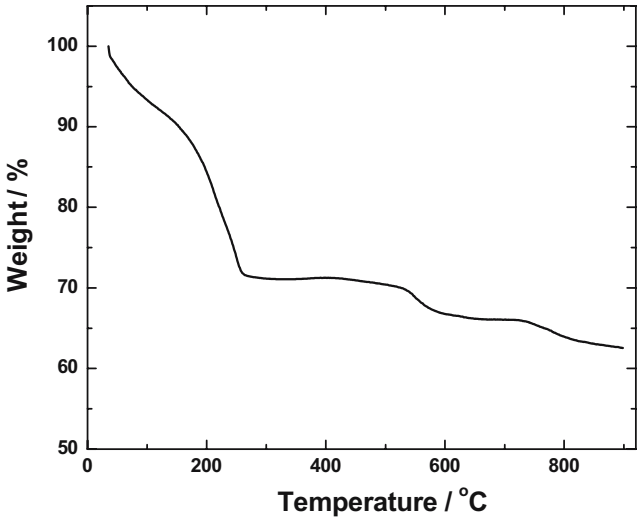


**Fig. 4** TGA of nanopetal α-$MnO_2$ recorded in air at a heating rate of 10 °C $min^{-1}$

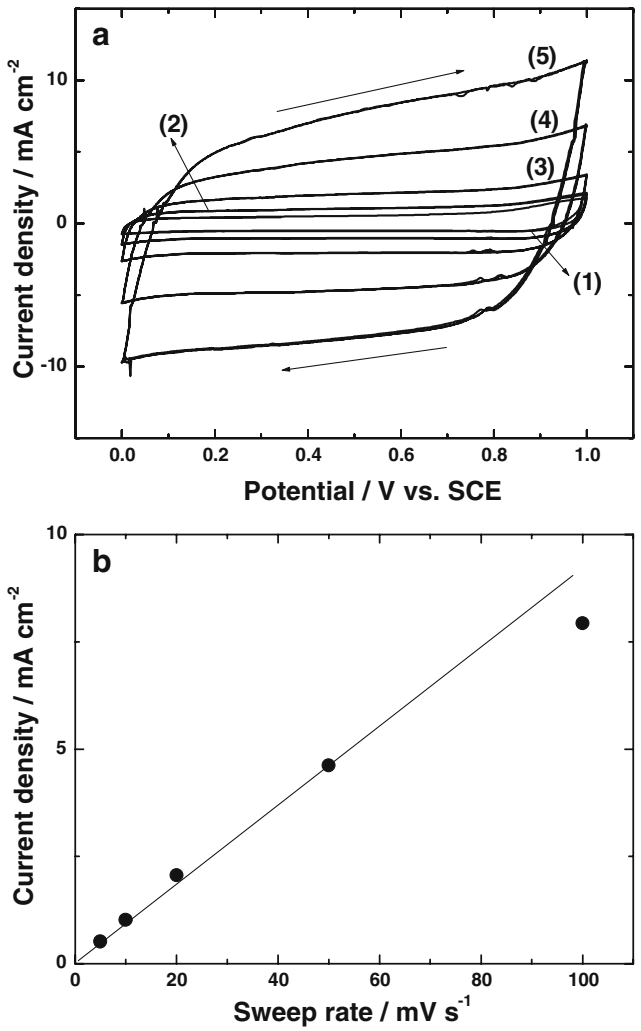


**Fig. 5** **a** Cyclic voltammograms of $MnO_2$ recorded at 5 (*1*), 10 (*2*), 20 (*3*), 50 (*4*), and 100 mV $s^{-1}$ (*5*) in 0.1 M $Na_2SO_4$. **b** Linear plot of voltammetric current density as a function of sweep rate

TGA thermogram and different phase transitions present in Fig. 4 are in agreement with the literature reported for $MnO_2$ [17].

Nanopetal α-$MnO_2$ electrodes were subjected to electrochemical studies in 0.1 M $Na_2SO_4$ aqueous electrolyte

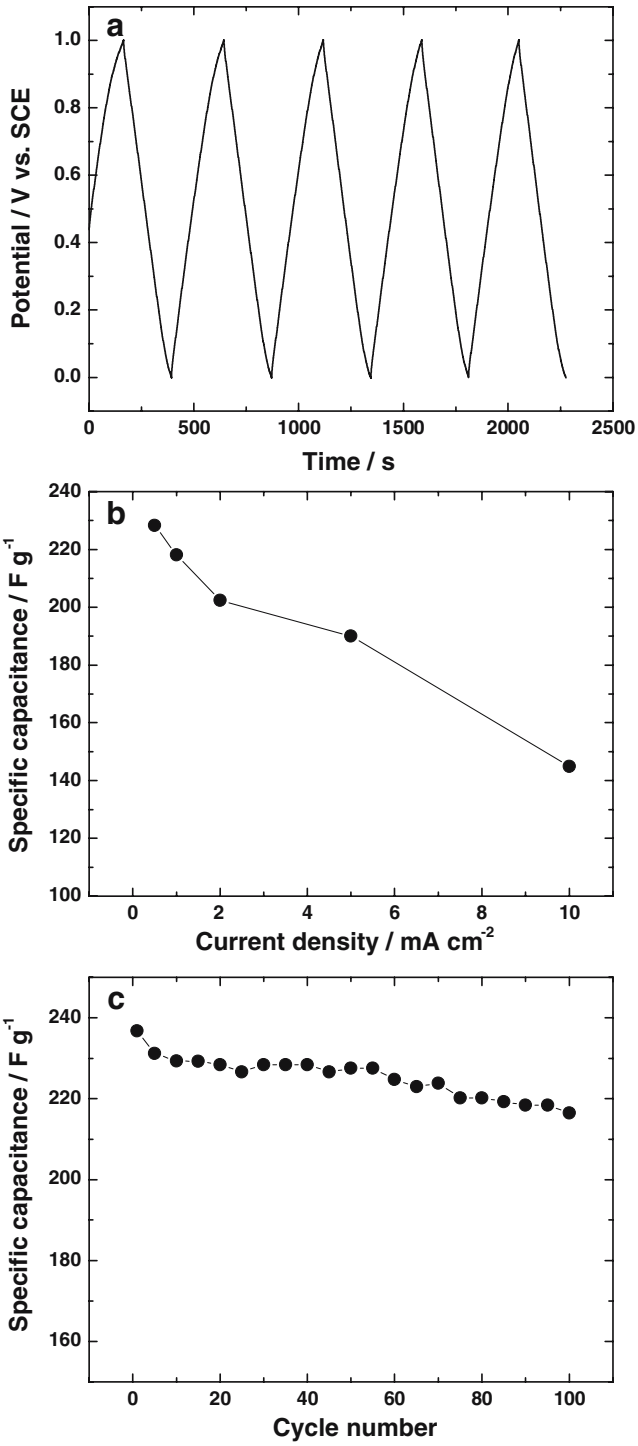


**Fig. 6** **a** Galvanostatic charge–discharge cycles recorded at 0.5 mA $cm^{-2}$ current density in 0.1 M $Na_2SO_4$, **b** dependence of specific capacitance on current density of galvanostatic charge–discharge cycling, and **c** cycling data at 0.5 mA $cm^{-2}$ for 100 cycles

[18]. Cyclic voltammograms recorded between 0 and 1.0 V at several sweep rates (Fig. 5a) exhibit rectangular shape. There is a linear increase in voltammetric current density with an increase in sweep rate (Fig. 5b), suggesting capacitive behavior of the electrodes. In addition to the existence of double-layer capacitance, $MnO_2$ possesses pseudocapacitance because of the reversible redox processes between $Mn^{4+}$ and $Mn^{3+}$. This process is accompanied by reversible insertion/deinsertion of alkali cation ($Na^+$) and/or proton ($H^+$) present in the electrolyte [19].

$$MnO_2 + Na^+ + e^- \rightleftharpoons MnOONa \quad (3)$$

Specific capacitance of the electrode was measured by conducting constant current charge–discharge cycling of the electrodes. Typical cycling curves showing variation of electrode potential with time of cycling at a current density (c.d.) of 0.5 mA $cm^{-2}$ are shown in Fig. 6a. There is a linear variation of potential during both charging and discharging processes. Specific capacitance (SC) is calculated using Eq. 4:

$$SC = It/(\Delta Em) \quad (4)$$

where $I$ is the discharge (or charge) current, $t$ is the time of discharge (or charge), $\Delta E$ (=1.0 V) is the potential window of cycling, and $m$ is the mass of $MnO_2$. Discharge SC obtained from the second cycle (Fig. 6a) is 228.3 F $g^{-1}$. As the SC of charging process is 240.2 F $g^{-1}$, the coulombic efficiency of charge–discharge cycling is 0.95 at a c.d. of 0.5 mA $cm^{-2}$. Cycling of the $\alpha$-$MnO_2$ electrodes were performed at several c.d.'s in the range from 0.5 to 10 mA $cm^{-2}$. The variation of SC with c.d. is shown in Fig. 6b. There is a decrease in SC with increase in c.d., which is due to a decrease in efficiency of utilization of the active material. Nevertheless, coulombic efficiency remained at 0.95–0.96 at all c.d.'s used for the experiments. The SC obtained is fairly constant during an extending charge–discharge cycling as shown in Fig. 6c.

## Conclusions

$MnO_2$ synthesized from a redox reaction between $KMnO_4$ and $MnSO_4$ in a microemulsion medium consisting of sodium dodecyl sulphate crystallizes in nanopetals morphology with $\alpha$ crystallographic structure. The electrochemical properties of $\alpha$-$MnO_2$ in 0.1 M $Na_2SO_4$ medium support its use for supercapacitor application. High values of specific capacitance are obtained.

**Acknowledgments** Authors thank Dr. H. N. Vasan for discussions, Mr. P. Ragupathy for XRD, and Mr. K. C. Suresh for surface area measurements. One of the authors (SD) acknowledges the senior research fellowship from the Council of Scientific and Industrial Research, New Delhi, India.

## References

1. Edelstein AS, Cammarata RC (1996) Nanomaterials: synthesis, properties and applications. Institute of Physics, Bristol and Philadelphia
2. Wu Y, Yang B, Zong B, Sun H, Shen Z, Feng Y (2004) J Mater Chem 14:469
3. Wu Y, Qiao P, Chong T, Shen Z (2002) Adv Mater 14:64
4. Na HT, Li J, Smith MK, Nguyen P, Cassell A, Han J, Meyyappan M (2003) Science 300:1249
5. Gautam UK, Vivekchand SRC, Govindaraj A, Rao CNR (2005) Chem Commun 3995
6. Zhang H, Yang D, Ma X, Ji Y, Xu J, Que D (2004) Nanotechnology 15:622
7. Conway BE (1999) Electrochemical supercapacitors. Kluwer, New York
8. Sarangapani S, Tilak BV, Chen CP (1996) J Electrochem Soc 143:3791
9. Zheng JP, Jow TR (1995) J Electrochem Soc 142:L6
10. Toupin M, Brousse T, Belanger D (2002) Chem Mater 14:3946
11. Wang X, Wang X, Huang W, Sebastian PJ, Gamboa S (2005) J Power Sources 140:211
12. Rodrigues S, Munichandraiah N, Shukla AK (1998) J Appl Electrochem 28:1235
13. Lee HY, Goodenough JB (1999) J Solid State Chem 144:220
14. Subramanian V, Zhu H, Vajtai R, Ajayan PM, Wei B (2005) J Phys Chem B 109:20207
15. Chen X, Li X, Jiang Y, Shi C, Li X (2005) Solid State Commun 136:94
16. Cushing BL, Kolesnichenko VL, O'Connor CJ (2004) Chem Rev 104:3893
17. Jeong YU, Manthiram A (2002) J Electrochem Soc 149:A1419
18. Devaraj S, Munichandraiah N (2005) Electrochem Solid-State Lett 8:A373
19. Toupin M, Brousse T, Belanger D (2004) Chem Mater 16:3184